Available online at www.sciencedirect.com
SCIENCE DIRECT
Journal of Solid State Chemistry 179 (2006) 1497–1505
JOURNAL OF SOLID STATE CHEMISTRY
www.elsevier.com/locate/jssc

A novel cobalt(II)–molybdenum(V) phosphate organic–inorganic hybrid polymer

Fa-Nian Shi[a], Filipe A. Almeida Paz[a], Penka I. Girginova[a], Helena I.S. Nogueira[a], João Rocha[a], Vítor S. Amaral[b], Jacek Klinowski[c], Tito Trindade[a,*]

[a]Department of Chemistry, CICECO, University of Aveiro, 3810-193 Aveiro, Portugal
[b]Department of Physics, CICECO, University of Aveiro, 3810-193 Aveiro, Portugal
[c]Department of Chemistry, University of Cambridge, Lensfield Road, Cambridge CB2 1EW, UK

Received 16 November 2005; received in revised form 1 February 2006; accepted 2 February 2006
Available online 10 March 2006

Abstract

A new organic–inorganic hybrid cobalt(II)–molybdenum(V) phosphate polymer incorporating piperazine (pip), $(H_2pip)_3[Co_3Mo_{12}O_{24}(OH)_6(PO_4)_8(H_{1.5}pip)_4]\cdot 5(H_2O)$, was prepared under hydrothermal conditions. As revealed by single-crystal X-ray diffraction studies, the material is modular, built from a secondary building block composed of two anionic hexameric polyoxomolybdophosphate $[Mo_6O_{12}(OH)_3(PO_4)_4]^{9-}$ moieties, bridged by a central octahedral Co^{2+} centre. The sandwich-type $\{Co[Mo_6O_{12}(OH)_3(PO_4)_4]_2\}^{16-}$ dimers are connected via tetrahedral Co^{2+} metal centres, forming an infinite one-dimensional polymer. The compound constitutes the first example of a reduced sandwich-type cobalt–molybdenum phosphate in which the organic moiety (pip) is effectively coordinated to the inorganic backbone of the polymer, in this case via the tetrahedrally coordinated Co^{2+} centres. The magnetic behaviour of this material was investigated in the temperature range 4–298 K.

Keywords: Hybrid material; Molybdenum phosphate; Polyoxometalates; Magnetochemistry

1. Introduction

Research in the area of organic–inorganic hybrid materials has attracted much interest in recent years owing to the structural diversity of these compounds associated to their potential applications in areas such as catalysis [1], gas sorption/storage [2], pharmaceutics [3], and emerging nanotechnologies [4]. Synthetic routes based on typical modular bottom-up approaches are very attractive as they tacitly give some control over the final topologies of these materials. In this context, well-defined inorganic clusters belonging to the polyoxometalate family are versatile structural units, which have been successfully used in self-assembling processes to produce functional polyoxometalate-based molecular materials [5].

A wide variety of molybdenum(V) phosphates have been reported in the literature [6–8]. Considering the pore size distribution in the regime of molecular-sized holes, as well as the thermochemical stability and the reactive sites, which lead to the possibility of achieving a high degree of chemical selectivity, these compounds have been described as embodying the attributes of "solid state inorganic enzymes" [6]. Their structure includes multinuclear molybdenum oxo-clusters ranging from around 30 to over 250 atoms, several of which are based on the hexameric anionic $[Mo_6O_{15}(HPO_4)(H_2PO_4)_3]^{5-}$ moiety ($[Mo_6P_4]$). This basic building unit can be further assembled, via an alkaline metal centre or a transition metal cation usually in the +2 oxidation state, into filled-sandwich secondary building units (SBUs) of the $M[Mo_6P_4]_2$ type.

Following our interest in the synthesis and structural characterisation of crystalline organic–inorganic hybrid materials [9] and polyoxometalates [10], we have decided to investigate the self-assembly of the $M[Mo_6P_4]_2$-type SBUs

*Corresponding author. Fax: +351 234 370 084.
E-mail address: ttrindade@dq.ua.pt (T. Trindade).

0022-4596/$ - see front matter © 2006 Elsevier Inc. All rights reserved.
doi:10.1016/j.jssc.2006.02.001

with organic molecules to produce new hybrid materials. So far, the known cobalt–molybdenum phosphates [8,11] do not contain the organic component chemically bound to the Co^{2+} centre, i.e. belonging to the first coordination sphere. The title compound, $(H_2pip)_3[Co_3Mo_{12}O_{24}(OH)_6(PO_4)_8(H_{1.5}pip)_4]\cdot 5(H_2O)$, constitutes the first example in which the tetrahedral Co^{2+} cations are effectively coordinated to piperazine (pip) moieties.

2. Experimental

All chemicals were readily available from commercial sources and were used as received without further purification. The synthesis was carried out in PTFE-lined stainless-steel reaction vessels (ca. 40 cm^3), under autogenous pressure and static conditions.

2.1. Synthesis of (H2pip)3[Co3Mo12O24(OH)6(PO4)8(H1.5pip)4]·5(H2O)

The title compound was synthesised from a reacting mixture containing 0.70 g of cobalt acetate tetrahydrate ($CoC_4H_6O_4\cdot 4H_2O$, 99.0% Fluka), 0.30 g of orthophosphoric acid (min. 85% H_3PO_4, Merck), 0.44 g of molybdenum trioxide (MoO_3, 99%, Aldrich) and 0.53 g of anhydrous pip ($C_4H_{10}N_2$, $\geqslant$98%, Merck-Schuchardt), in ca. 15 g of distilled water. The suspension was transferred to the reaction vessel and then placed inside a pre-heated oven at 200 °C. The reaction proceeded for 3 days, after which the reaction vessel was allowed to cool slowly to ambient temperature before opening. The autoclave contents consisted of a large amount of dark-red needle-like crystals, which were formulated as $(H_2pip)_3[Co_3Mo_{12}O_{24}(OH)_6(PO_4)_8(H_{1.5}pip)_4]\cdot 5(H_2O)$ on the basis of single-crystal X-ray diffraction, and a small amount of powdered impurities. The latter materials were readily separated from the single crystals by sonication (ca. 15 min), followed by filtration and washing with copious amounts of distilled water. The title compound proved to be air- and light-stable, and insoluble in water and common organic solvents.

2.2. Instrumentation

FT-IR spectra were collected using KBr pellets (Aldrich 99%+, FT-IR grade) on a Mattson 7000 FT-IR spectrometer. Thermogravimetric analyses (TGA) were carried out using a Shimadzu TGA 50, with a heating rate of 10 °C/min, under a continuous nitrogen stream with a flow rate of 20 cm^3/min. Elemental analyses for C, H and N were performed with a CHNS-932 Elemental analyser at the Microanalysis Laboratory at the University of Aveiro. Scanning Electron Microscopy (SEM) and Energy Dispersive analysis of X-ray Spectroscopy (EDS) studies were performed using a Hitachi S-4100 field emission gun tungsten filament instrument working at 25 kV. The measurements of magnetic susceptibilities of a powdered sample of the title compound were performed under variable temperature from 4.5 to 300 K using a Quantum Design Superconducting Quantum Interference Device (SQUID) magnetometer MPMS at the University of Porto (Portugal).

2.3. Single-crystal X-ray diffraction

A suitable single crystal of the title compound was mounted on a glass fibre using perfluoropolyether oil [12]. Data were collected at 180(2) K on a Nonius Kappa charge coupled device (CCD) area-detector diffractometer (Mo$K\alpha$ graphite-monochromated radiation, $\lambda = 0.7107$ Å), equipped with an Oxford Cryosystems cryostream and controlled by the collect software package [13]. Images were processed using the software packages of Denzo and Scalepack [14], and the data were corrected for absorption by the empirical method employed in Sortav [15]. The structure was solved by the direct methods of SHELXS-97 [16], and refined by full-matrix least-squares on F^2 using SHELXL-97 [17].

All non-hydrogen atoms were directly located from difference Fourier maps and, when possible, refined with anisotropic displacement parameters. Pip residues were refined with geometry heavily restrained in order to ensure a chemically reasonable geometry for these moieties: on the one hand, the C–N and C–C bond distances were restrained to 1.48(1) and 1.50(1) Å, respectively, and, on the other, the C···N and C···C distances across the cyclic chains were further restrained to a common distance factor which refined to ca. 2.46(1) Å. Even though hydrogen atoms associated with the nitrogen atoms of these moieties were usually visible in difference Fourier maps calculated from successive least-squares refinements, these atoms were added in idealised positions using appropriate *HFIX 13* and *23* instructions in SHELXL [17]. The hydrogen atoms were then allowed to ride on their parent atoms with an isotropic displacement parameter fixed at 1.2 of $U_{eq}(N)$. The three crystallographically unique uncoordinated piperazinium cations, H_2pip^{2+}, were found to be severely affected by thermal disorder, and all carbon and nitrogen atoms from each moiety were refined using a common isotropic displacement parameter (one parameter for each cation).

One cobalt centre was found to be disordered over two crystallographic generic positions, Co(2) and Co(2′), and modelled anisotropically with fixed rates of occupancy of 75% and 25%, respectively. Non-hydrogen atoms from the coordinated piperazinium cation to Co(2) refined successfully using anisotropic displacement parameters. The piperazinium cation, neighbouring Co(2′), was found to be disordered over two different crystallographic positions, which were modelled with fixed rates of occupancy of 50% each, and using isotropic displacement parameters for all non-hydrogen atoms belonging to the same moiety (one parameter for each disordered piperazinium cation). To balance the crystal charge, it is feasible to assume that these

Table 1
Crystal data and structure refinement information

Formula	$C_{28}H_{98}Co_3Mo_{12}N_{14}O_{67}P_8$
Formula weight	3279.03
Crystal system	Triclinic
Space group	$P\bar{1}$
a (Å)	13.856(3)
b (Å)	13.884(3)
c (Å)	14.410(3)
α (deg)	83.99(3)
β (deg)	69.40(3)
γ (deg)	61.17(3)
Volume (Å^3)	2266.1(8)
Z	1
D_c (g/cm^3)	2.403
μ(Mo$K\alpha$) (mm^{-1})	2.389
F (000)	1604
Crystal size (mm)	$0.35 \times 0.12 \times 0.02$
Crystal type	Red blocks
θ range	3.52–25.05
Index ranges	$-16 \leqslant h \leqslant 16$
	$-16 \leqslant k \leqslant 16$
	$-16 \leqslant l \leqslant 17$
Reflections collected	18362
Independent reflections	7944 ($R_{int} = 0.0564$)
Final R indices [$I > 2\sigma(I)$]	$R_1 = 0.0701$
	w$R_2 = 0.1698$
Final R indices (all data)	$R_1 = 0.1117$
	w$R_2 = 0.1943$
Largest diff. peak and hole	3.189 and -1.332 e Å^{-3}

Table 2
Selected bond lengths (Å) for $(H_2pip)_3[Co_3Mo_{12}O_{24}(OH)_6(PO_4)_8(H_{1.5}pip)_4] \cdot 5(H_2O)$[a]

Mo(1)–O(2)	1.976(8)	Mo(4)–O(3)	1.966(8)
Mo(1)–O(4)	2.279(8)	Mo(4)–O(6)	2.221(8)
Mo(1)–O(17)	2.049(10)	Mo(4)–O(12)	2.058(10)
Mo(1)–O(20)	2.075(9)	Mo(4)–O(26)	1.938(8)
Mo(1)–O(21)	1.682(9)	Mo(4)–O(27)	1.684(9)
Mo(1)–O(22)	1.946(8)	Mo(4)–O(28)	2.103(8)
Mo(2)–O(2)	1.983(7)	Mo(5)–O(1)	1.967(8)
Mo(2)–O(5)	2.308(8)	Mo(5)–O(6)	2.265(8)
Mo(2)–O(8)	2.038(8)	Mo(5)–O(13)	2.042(9)
Mo(2)–O(23)	1.681(9)	Mo(5)–O(28)	2.082(9)
Mo(2)–O(22)	1.945(10)	Mo(5)–O(29)	1.678(8)
Mo(2)–O(24)	2.075(9)	Mo(5)–O(30)	1.921(9)
Mo(3)–O(3)	1.974(7)	Mo(6)–O(31)	1.686(9)
Mo(3)–O(5)	2.277(8)	Mo(6)–O(1)	1.975(8)
Mo(3)–O(9)	2.025(8)	Mo(6)–O(4)	2.300(8)
Mo(3)–O(24)	2.079(9)	Mo(6)–O(16)	2.054(10)
Mo(3)–O(25)	1.691(9)	Mo(6)–O(20)	2.063(10)
Mo(3)–O(26)	1.935(9)	Mo(6)–O(30)	1.941(9)
Co(2)–O(7)	1.972(8)	Co(2′)–O(7)	2.031(10)
Co(2)–O(11)^{i}	1.836(10)	Co(2′)–O(11)^{i}	1.959(10)
Co(2)–O(15)	1.931(9)	Co(2′)–O(15)	1.946(12)
Co(2)–N(1)	2.063(9)	Co(2′)–N(5)	2.41(2)
		Co(2′)–N(8)	2.02(3)
Co(1)–O(1)	2.126(8)		
Co(1)–O(2)	2.209(7)		
Co(1)–O(3)	2.103(7)		

[a]Symmetry transformation used to generate equivalent atoms: (i) $2-x$, $-y$, $1-z$.

Table 3
Selected bond angles (deg) for the Co^{2+} coordination environments present in $(H_2pip)_3[Co_3Mo_{12}O_{24}(OH)_6(PO_4)_8(H_{1.5}pip)_4] \cdot 5(H_2O)$[a]

O(1)–Co(1)–O(2)	94.1(3)	O(3)–Co(1)–O(2)	94.5(3)
O(1)–Co(1)–O(2)^{ii}	85.9(3)	O(3)–Co(1)–O(1)^{ii}	83.8(3)
O(3)–Co(1)–O(1)	96.2(3)	O(3)–Co(1)–O(2)^{ii}	85.5(3)
O(7)–Co(2)–N(1)	114.8(4)	O(11)^{i}–Co(2)–N(1)	107.8(4)
O(11)^{i}–Co(2)–O(7)	103.3(4)	O(15)–Co(2)–O(7)	115.2(4)
O(11)^{i}–Co(2)–O(15)	111.8(5)	O(15)–Co(2)–N(1)	104.0(4)
O(7)–Co(2′)–N(5)	94.0(8)	O(15)–Co(2′)–O(11)^{i}	106.0(5)
O(11)^{i}–Co(2′)–O(7)	97.0(5)	O(15)–Co(2′)–N(5)	135.8(8)
O(11)^{i}–Co(2′)–N(5)	105.6(8)	O(15)–Co(2′)–N(8)	108.0(11)
O(11)^{i}–Co(2′)–N(8)	119.8(12)	N(8)–Co(2′)–O(7)	113.7(11)
O(15)–Co(2′)–O(7)	111.9(5)	N(8)–Co(2′)–N(5)	28.0(12)

[a]Symmetry transformations used to generate equivalent atoms: (i) $2-x$, $-y$, $1-z$; (ii) $2-x$, $-y$, $-z$.

two piperazinium moieties should be double protonated when not coordinated to the cobalt centres. Hence, per formula unit, an average charge of -1 is thus compensated by the presence of a hydrogen atom statistically distributed among the coordinating nitrogen donor atoms.

Hydrogen atoms attached to carbon were located at their idealised positions using the *HFIX 23* instruction in SHELXL [17], and included in the refinement in riding-motion approximation with an isotropic thermal displacement parameter fixed at 1.2 times U_{eq} of the carbon atom to which they are attached. Five water molecules of crystallisation were directly located from difference Fourier maps and refined with a common isotropic displacement parameter and fixed site occupancy of 50%.

Hydrogen atoms associated with protonated OH bridges in the $\{Mo_6O_{12}(OH)_3\}$ moieties, as described by Sécheresse and collaborators [18], were also not clearly visible in difference Fourier maps. Just like for the hydrogen atoms associated with the water molecules of crystallisation, no attempt was made to place these hydrogen atoms in calculated positions, but they have all been included in the empirical formula of the compound (see Table 1). The last difference Fourier map synthesis showed the highest peak (3.189 e Å^{-3}) located at 1.42 Å from P(4), and the deepest hole (-1.332 e Å^{-3}) at 0.74 Å from Mo(6).

Information concerning crystallographic data collection and structure refinement details are summarised in Table 1.

Selected bond lengths and angles are given in Tables 2 and 3, respectively. Hydrogen bonding geometry is described in Table 4. Crystallographic data (excluding structure factors) for the structure reported in this paper have been deposited with the Cambridge Crystallographic Data Centre as supplementary publication no. CCDC-289064. Copies of the data can be obtained free of charge on application to CCDC, 12 Union Road, Cambridge CB2 2EZ, UK (fax: +44 1223 336033; e-mail: deposit@ccdc.cam.ac.uk).

3. Results and discussion

The title compound was obtained as a single-crystalline pure phase using a typical hydrothermal synthetic approach. By varying the molar ratios between reagents, different phases (and their relative quantity) have been systematically obtained. However, a phase-pure material of the title compound was never directly isolated from the autoclave contents. The chemical composition given in the experimental section for the starting reactive mixture is that which minimises the amount of unknown powdered impurities. Nevertheless, single crystals of the title compound could easily be manually harvested due to the macroscopic characteristics such as crystal size, morphology and red colour.

Table 4
Hydrogen bonding geometry (distances in Å and angles in degrees) for $(H_2pip)_3[Co_3Mo_{12}O_{24}(OH)_6(PO_4)_8(H_{1.5}pip)_4]\cdot 5(H_2O)$[a]

D–H···A	$d(D\cdots A)$	$<(DHA)$
N(1)–H(1)···O(26)	2.744(13)	150.7
N(2)–H(2A)···O(18)^{i}	2.803(15)	177.0
N(2)–H(2B)···O(22)^{ii}	2.796(15)	170.1
N(3)–H(3C)···O(25)^{iii}	2.87(2)	148.5
N(3)–H(3D)···O(19)	2.63(2)	169.4
N(4)–H(5C)···O(29)	3.21(2)	132.9
N(4)–H(5D)···O(31)^{iv}	3.06(2)	125.4
N(7)–H(7A)···O(21)^{v}	2.80(4)	139.0
N(7)–H(7B)···O(14)	2.75(4)	166.8
N(6)–H(6C)···O(18)	3.17(3)	145.1
N(6)–H(6D)···O(14)^{vi}	3.07(3)	128.0
N(8)–H(8)···O(30)	2.90(4)	150.0
N(9)–H(9C)···O(15)^{vi}	2.94(4)	160.9
N(9)–H(9D)···O(1W)^{vi}	2.97(4)	171.7

[a]Symmetry transformations used to generate equivalent atoms: (i) $1+x$, y, z; (ii) $2-x$, $-y$, $1-z$; (iii) $2-x$, $-y$, $-z$; (iv) $1-x$, $1-y$, $-z$; (v) x, $1+y$, z; (vi) $1-x$, $1-y$, $1-z$.

The isolated single crystals appear as long hexagonal and tubular needles, as shown in the SEM picture given as Fig. 1. This morphology facilitates a preferential orientation of the crystallites when they are placed on a flat substrate, hence explaining the relative strong reflections observed in the X-ray diffraction pattern of the compound (Supplementary material).

X-ray diffraction studies on a handful of single crystals isolated from different batches revealed that the title compound is composed of anionic $[(Mo_2^{V}O_4)_3(\mu_2\text{-}OH)_3(\mu_2\text{-}PO_4)_3(\mu_6\text{-}PO_4)]^{9-}$ units (or $[Mo_6O_{12}(OH)_3(PO_4)_4]^{9-}$, abbreviated to $[Mo_6P_4]$) as the primary building blocks of the polymer (Fig. 2). As observed for some related structures [19], this building unit has a C_3 symmetry through a three-fold axis containing the geometrical centre of the moiety and perpendicular to the plane of the Mo^{5+} centres. It can be found in several Mo^{5+} phosphate compounds [6–8,18,20], and is closely related to the structure of a number of polyoxomolybdenum(V) clusters containing organophosphonate ligands [21], as sulphite [22], sulphate/arsenite [23] and carbonate groups [19]. Moreover, these complexes are structurally related to the Anderson polyoxoanions of the $[XMo_6O_{24}]^{n-}$ type, which also show a Mo_6 planar ring with a central octahedral coordination position occupied by an heteroatom ($X = I$, Te, Fe or Al) [24].

The anionic $[Mo_6P_4]$ hexamer is formed by edge-sharing [via the μ_2-OH^- and μ_2–PO_4^{3-}—see Fig. 2] of three crystallographic independent $\{Mo_2^{V}O_4\}^{2+}$ fragments [Mo(1–2), Mo(3–4) and Mo(5–6), also structurally formed by edge-sharing via μ_2-O^{2-}—see Fig. 2], leading to an hexamer in which the Mo···Mo distances across the ring form two alternating families of distances. From Mo(1) to Mo(6), back

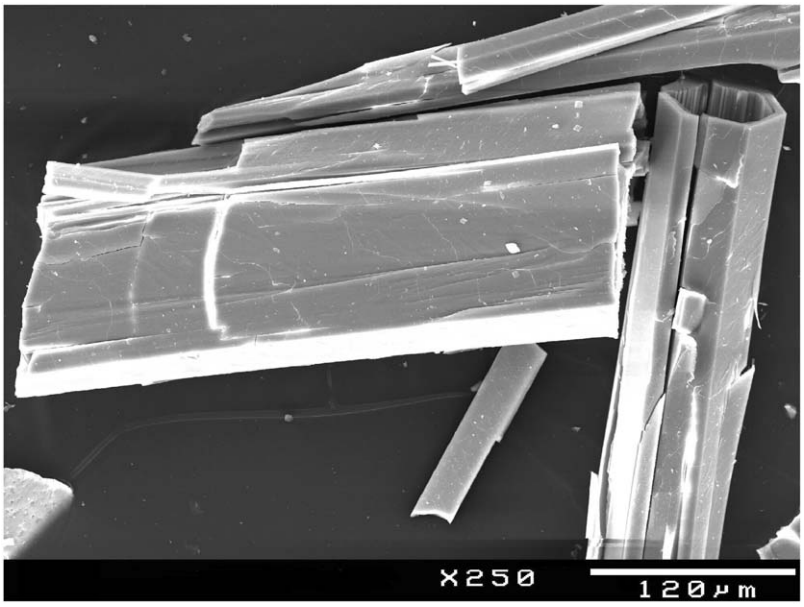

Fig. 1. SEM image of hexagonal tubular single crystals of $(H_2pip)_3[Co_3Mo_{12}O_{24}(OH)_6(PO_4)_8(H_{1.5}pip)_4]\cdot 5(H_2O)$.

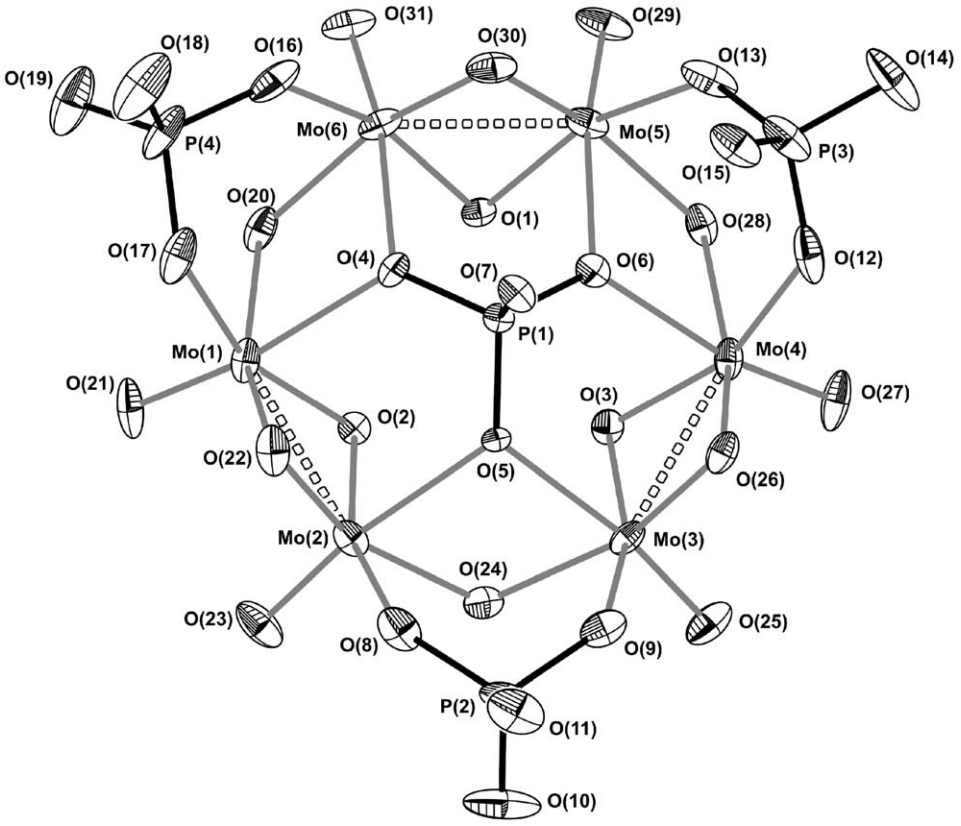

Fig. 2. Schematic representation of the anionic $[Mo_6O_{12}(OH)_3(PO_4)_4]^{9-}$ hexamer with thermal ellipsoids drawn at the 30% probability level. Mo···Mo interactions are represented as dashed white-filled bonds: Mo(1)···Mo(2) 2.596(2) Å, Mo(3)···Mo(4) 2.605(2) Å, Mo(5)···Mo(6) 2.589(2) Å. For selected bond lengths and angles see Tables 2 and 3, respectively.

to Mo(1) the inter-metallic separations are of 2.596(2), 3.460(2), 2.605(2), 3.462(2), 2.589(2) and 3.461(2) Å, respectively. The shorter Mo···Mo distances [in the range 2.589(2)–2.605(2) Å] correspond to typical bonding interactions between the involved Mo^{5+} centres, and are a consequence of the combined effect of the rather short Mo–(μ_2-O) bonds [in the range 1.921(9)–1.983(7) Å] and small Mo–(μ_2-O)–Mo bite angles [in the range 82.0(3)–84.5(3)]. It is interesting to note that these binuclear moieties can also be found as a structural element (linker-groups) in mixed-valence molybdenum-oxide-based giant spheres and baskets, as reported by Müller and collaborators [25].

The six crystallographically independent Mo^{5+} centres appear in a highly distorted octahedral coordination environment, $\{MoO_6\}$, being coordinated to two phosphate ligands [one peripheral μ_2-bridging and the central μ_6-bridging P(1)], one terminal oxo group, one μ_2-OH^- plus two μ_2-O^{2-} (Fig. 2). It is interesting to note that the terminal Mo=O group [bond lengths in the range 1.678(8)–1.691(9) Å—see Table 2] is, for all Mo^{5+} centres, apical to the coordinating μ_6-bridging phosphate [Mo–O bond distance in the range 2.221(8)–2.308(8) Å—see Table 2], markedly exerting its *trans* effect in the latter bond lengths. Such effect is also reflected in the average displacement of the metallic centres (above the equatorial plane of the octahedra) of about 0.37 Å towards the oxo groups. The equatorial planes of the $\{MoO_6\}$ octahedra are composed of the μ_2-O^{2-} oxo, μ_2-OH^- and μ_2-bridging phosphate groups with the Mo–O bond lengths found within the range 1.935(9)–2.103(8) Å.

Four crystallographically independent phosphate groups decorate the $[Mo_6P_4]$ anionic unit: one is positioned in the centre of the moiety [P(1)] bridging the six Mo^{5+} centres, and the remaining three are peripheral to the hexamer, interconnecting the $\{Mo_2^{V}O_4\}^{2+}$ fragments [P(2), P(3) and P(4)] (Fig. 2). The P–O bond lengths and O–P–O bond angles are found within the ranges 1.514(10)–1.578(12) Å and 104.4(7)–112.8(6)°, respectively, values which are comparable with those typically found in related compounds.

The material contains two crystallographically independent Co^{2+} centres, Co(1) and Co(2), which have different, but complementary, structural functionality. Co(1) interconnects two adjacent anionic $[Mo_6P_4]$ hexamers via the bridging O(1–3) oxo groups (Fig. 2), leading to the formation of an anionic sandwich-type cluster, $[CoMo_{12}O_{24}(OH)_6(PO_4)_8]^{16-}$, which can be seen as the SBU for the construction of the one-dimensional polymer. This Co^{2+} centre appears with a coordination geometry resembling a slightly distorted octahedron, $\{CoO_6\}$, with the bond lengths and octahedral *cis* angles found within the

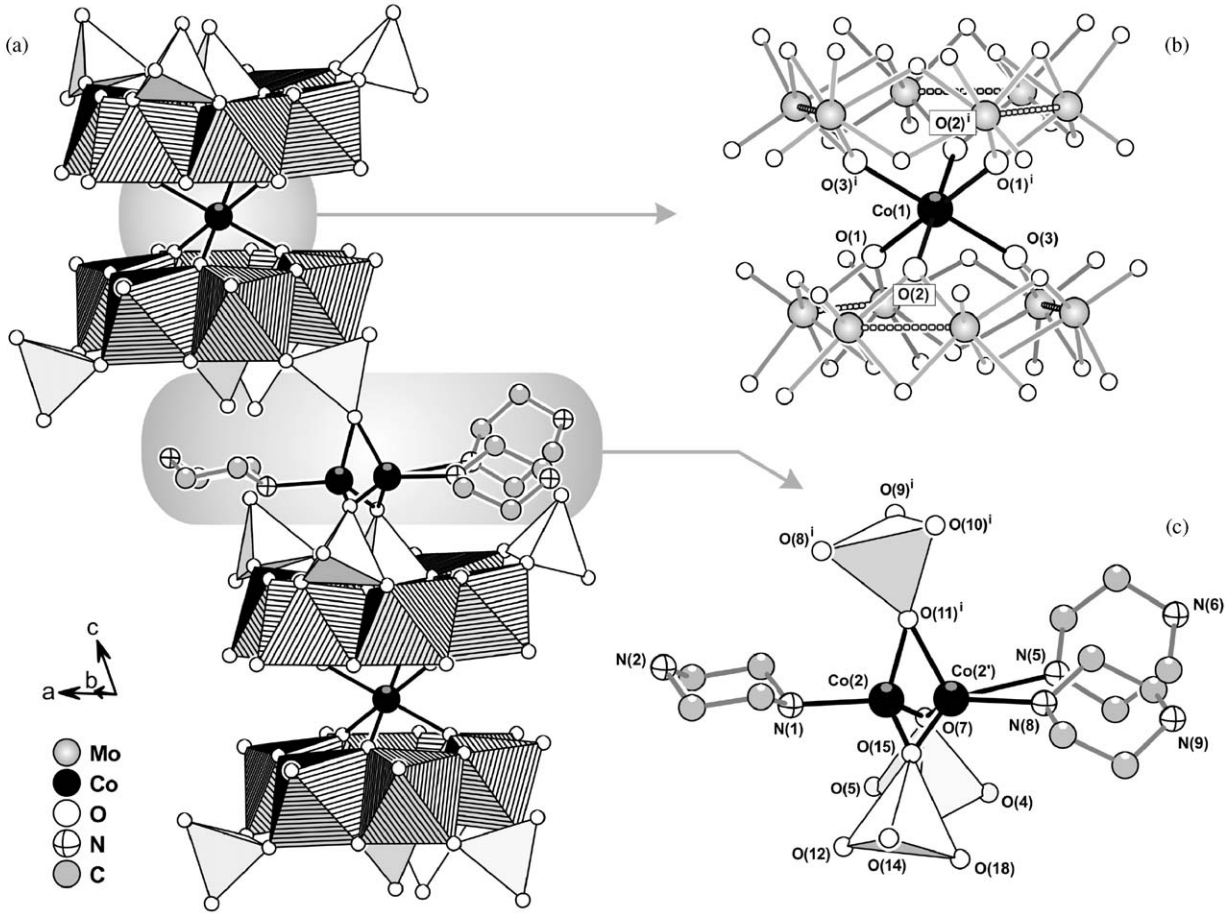

Fig. 3. (a) Schematic representation of two consecutive sandwich-type $[Mo_6O_{12}(OH)_3(PO_4)_4]^{9-}$ SBUs of the anionic one-dimensional polymer $[Co_3Mo_{12}O_{24}(OH)_6(PO_4)_8(H_{1.5}pip)_4]_n^{6n-}$ present in the title compound. The local coordination environments of (b) Co(1) and (c) Co(2) and Co(2′) are also depicted. For selected bond lengths and angles see Tables 2 and 3, respectively. Hydrogen atoms have been omitted for clarity. Symmetry code used to generate equivalent atoms: (i) $2-x, -y, -z$.

ranges 2.103(7)–2.209(7) Å and 83.8(3)–96.2(3)°, respectively (Fig. 3 and Tables 2 and 3). The second type of Co^{2+} centre is coordinated to pip residues, and also interconnects adjacent SBUs as depicted in Fig. 3 [the O(11)-donor atom from one SBU is bridged to O(7) and O(15) via the Co^{2+} centre] leading to the formation of a one-dimensional anionic polymer, $[Co_3Mo_{12}O_{24}(OH)_6(PO_4)_8(H_{1.5}pip)_4]_n^{6n-}$, running parallel to the *c*-axis. It is interesting to note that the latter metallic centre appears disordered over two distinct crystallographic positions, Co(2) and Co(2′), with refined rates of occupancy of 3:1, respectively. For the two cobalt positions the coordination geometry resembles that of a tetrahedron, $\{CoO_3N\}$, which was found to be significantly more regular for Co(2) [bond lengths and angles within the ranges 1.836(10)–2.063(9) Å and 103.3(4)–115.2(4)°]. As represented in Fig. 3, the coordination sphere of Co(2′) is appreciably affected by disorder, with the coordinated protonated pip residue being refined over two distinct crystallographic positions.

Uncoordinated pip residues appear in the title material not only as space-fillers, but also as charge-compensating moieties through protonation of the nitrogen atoms. These moieties, along with the water molecules of crystallisation, are in turn involved in a strong and very extensive hydrogen bonding sub-network (Fig. 4 and Table 4) which further stabilises the above-described anionic $[Co_3Mo_{12}O_{24}(OH)_6(PO_4)_8(H_{1.5}pip)_4]_n^{6n-}$ coordination polymer in the solid state.

The CHN elemental composition and infrared vibrational data (summarised in Table 5) further support the chemical composition and structural details described by the crystallographic studies. In particular, the IR spectrum of the compound provides strong bands at 956 and 722–741 cm^{-1}, assigned to characteristic vibrational modes of $[Mo_6P_4]$ hexamers, confirming their integrity in the final compound. The thermal stability of $(H_2pip)_3[Co_3Mo_{12}O_{24}(OH)_6(PO_4)_8(H_{1.5}pip)_4]\cdot 5(H_2O)$ compound was tested between ambient temperature and 1000 °C, with the thermogram showing three main weight losses. The first continuous weight loss occurs in the temperature range 48–103 °C (ca. 2.6%), and agrees well with the release of all five water molecules of crystallisation (calculated weight loss of ca. 2.7%). The second weight loss, registered in the temperature range 103–651 °C, is attributed to the partial

thermal decomposition of the organic component, with the observed weight loss (ca. 13.9%) being consistent with the release of approximately five pip residues (calculated value of ca. 13.1%). Interestingly, this seems to suggest that, most probably, the disorder around the Co(2) centre disappears, with one organic moiety being retained in the structure so as to complete (and stabilise) the coordination sphere of such metallic centre. Further weight losses up to 1000 °C are attributed to the thermal decomposition of the remnant organic component, leading to the formation of the inorganic cobalt molybdenum phosphate ($Co_3Mo_9O_{20}(P_2O_7)_4$) (observed and calculated final residues of ca. 63.5% and 62.7%, respectively).

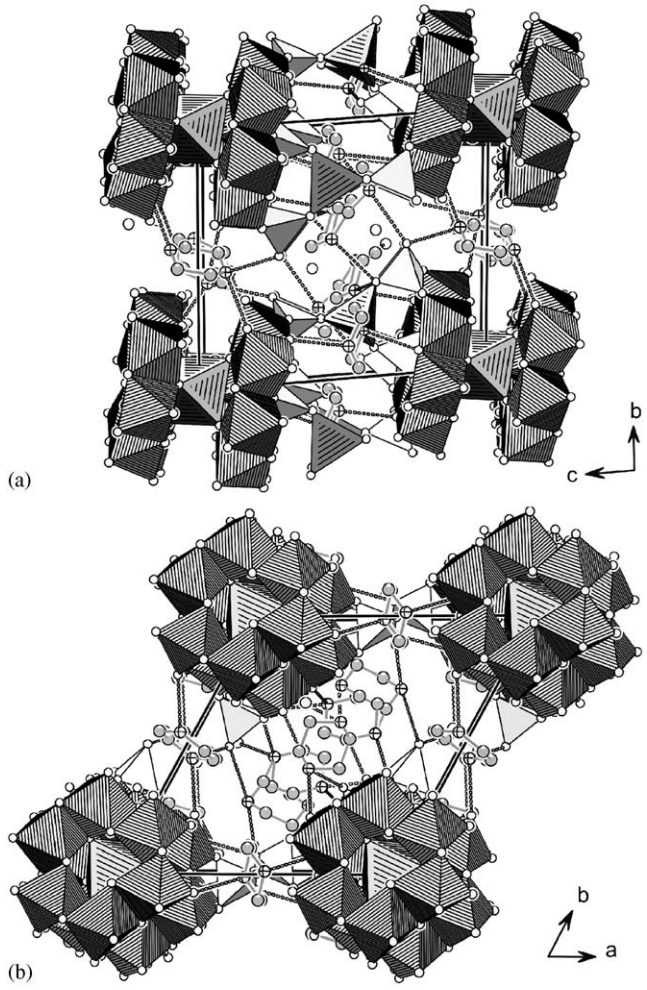

Fig. 4. Crystal packing of $(H_2pip)_3[Co_3Mo_{12}O_{24}(OH)_6(PO_4)_8(H_{1.5}pip)_4]\cdot 5(H_2O)$ viewed along the (a) [100] and (b) [001] directions of the unit cell. The one-dimensional hybrid polymers are represented with polyhedra for the Mo, Co and P centres, piperazine residues are represented in ball-and-stick mode, and hydrogen bonding interactions involving the N-donor atoms from these moieties are drawn as white-filled dashed lines. For hydrogen bonding details see Table 4. Hydrogen atoms have been omitted for clarity.

Magnetic data for a powdered sample of $(H_2pip)_3[Co_3Mo_{12}O_{24}(OH)_6(PO_4)_8(H_{1.5}pip)_4]\cdot 5(H_2O)$ was collected in the temperature (T) range 4.5–300 K in an applied magnetic field of 100 Oe. The analysis of the data shows that there are two temperature regions with distinct behaviours. In the temperature range 150–300 K the experimental data for the magnetic susceptibility obeys the Curie law for non-interacting ions, $\chi_m = C/T$, where C is the Curie constant. This can be seen in Fig. 5, where the temperature dependence of the inverse of the magnetic susceptibility χ_m per molar molecular unit of $(H_2pip)_3[Co_3Mo_{12}O_{24}(OH)_6(PO_4)_8(H_{1.5}pip)_4]\cdot 5(H_2O)$ is presented. The inset shows the plot $\chi_m T$ vs. T. The dashed line through the origin in Fig. 5 and the constant portion of $\chi_m T$ characterise the data between 150 and 300 K.

From the Curie constant an effective magnetic moment $\mu_{eff} = 4.82\,\mu_B$ per Co ion was obtained, which is in agreement with the magnetic moment reported for Co(II) in a high-spin ($S = 3/2$) state [26,27]. This result also indicates that the d^1 electrons in the Mo(V) cations are coupled and have no net contribution to the magnetic moment of compound $(H_2pip)_3[Co_3Mo_{12}O_{24}(OH)_6(PO_4)_8(H_{1.5}pip)_4]\cdot 5(H_2O)$.

At 150 K, a sudden change from the typical Curie law was observed (inset of Fig. 5), and at lower temperature the magnetic moment (μ_{eff}) slightly increased ($\mu_{eff} = 4.90\,\mu_B$ per ion); the susceptibility shows mainly antiferromagnetic interactions between the Co(II) ions. Fig. 6 shows the temperature dependence of χ_m. The low temperature details (insets a and b) show that near 10 K, χ_m appears to diverge, with a minimum slope $d\chi_m/dT$ indicating a magnetic transition, a behaviour analogous to that observed in ferrimagnets and weak ferromagnets. Therefore, the magnetic susceptibility was modelled considering the competition of antiferromagnetic and ferromagnetic interactions in a system of two ion lattices, that we associate with the two types of Co ions, one for Co(1) in octahedral coordination and the other for Co(2) and Co(2′) in tetrahedral coordination.

Table 5
CHN elemental composition (calculated values are given inside the parentheses) and vibrational spectroscopic data for $(H_2pip)_3[Co_3Mo_{12}O_{24}(OH)_6(PO_4)_8(H_{1.5}pip)_4]\cdot 5(H_2O)$

Elemental composition (%)			Vibrational data (cm^{-1})										
C	N	H	ν(O–H)	ν(N–H)	ν_{asym}(C–H)	ν_{sym}(C–H)	ν(N^+–H)	δ(H–O–H)	ν(C–C)	ν(C–N)	ν(P–O)	ν(Mo–O)	ν(Mo–O–M)
9.53	5.49	2.96	3477s, b	3254s, b	3041m	2830m	2500–2300w, b	1638s	1462s		1092s		741s
(10.27)	(5.99)	(2.75)			3031m	2785m			1403m		1038s	956vs	
									1341w				722s

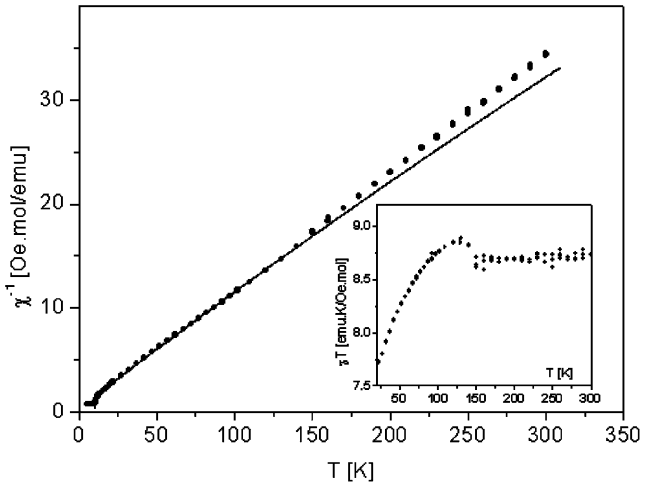

Fig. 5. (a) Temperature dependence of the inverse molar magnetic susceptibility. Solid line: ferrimagnetic fit described in text. Dashed line: high temperature behaviour. Inset: temperature of the molar magnetic susceptibility multiplied by temperature, showing the change of behaviour at $T \sim 140$ K.

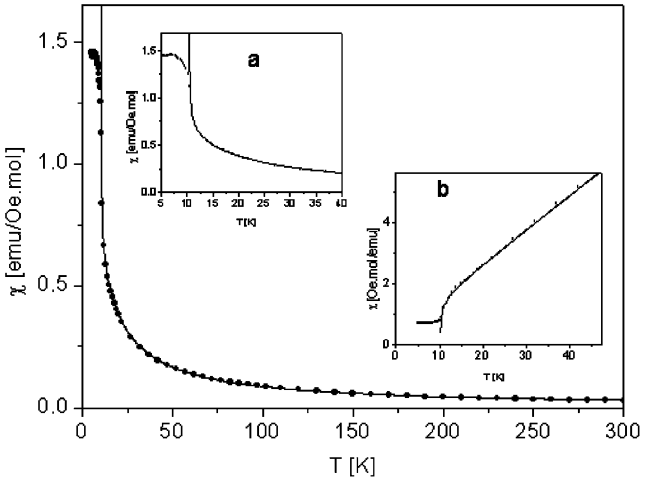

Fig. 6. Temperature dependence of the molar magnetic susceptibility. Solid line: fit to a ferrimagnetic behaviour. Inset (a) low temperature detail. Inset (b) plot of the inverse molar magnetic susceptibility vs. temperature.

We consider the existence of antiferromagnetic interactions (W_{12}) between ions of different type (1 with 2 and 2′, mediated by the Mo rings) and ferromagnetic between ions of the same type (W_{11} and W_{22}). In the interval from 10.5 to 130 K, χ_m was fitted to a simple mean field expression (the Néel hyperbola) [28,29] with an additional residual temperature independent term, χ_0:

$$\chi_m^{-1} = \frac{T+\theta_p}{C} - \frac{\gamma}{T-\theta}, \quad (1)$$

C is the Curie constant, with the temperatures θ_p and θ defining the asymptotes. The fitted curve, which follows the data quite well (χ^2 error $= 8 \times 10^{-6}$) is represented as a solid line in Figs. 5 and 6. From the fitting one obtains $C = 8.70$ emuK/Oe mol, $\theta_p = -3.3$ K, $\theta = 9.65$ K and $\chi_0 = 0.0023$ emu/Oe mol. These values and γ show that the ferromagnetic interactions are a fraction of the antiferromagnetic: $W_{11} = 0.66|W_{12}|$ and $W_{22} = 0.32|W_{12}|$. From this model χ_m should also diverge at a critical temperature $T_C = 10.0$ K (insets in Fig. 6).

As described above, $(H_2pip)_3[Co_3Mo_{12}O_{24}(OH)_6(PO_4)_8(H_{1.5}pip)_4] \cdot 5(H_2O)$ has a chain framework with Co(II) ions (Co1, Co2 and Co2′, in Fig. 3) bridging hexa-Mo rings. The shortest Co···Co distance is ca. 6.65 Å along the chain direction and 5.94 Å perpendicular to the chain direction. The antiferromagnetic–magnetic interactions observed below 150 K are presumably due to the super-exchange coupling among Co^{2+} mediated through O–Mo–O–P–O chains. At the moment we can only speculate that probably the Mo(V) ions become polarised at 150 K due to slight structural modifications. On the other hand, the positive interactions W_{11} and W_{22} can be due to superexchange across ligands or to anisotropic exchange interactions of the Dzyalozinsky–Moryia type (weak ferromagnetism) [28]. To the best of our knowledge, this is the first report of coexisting antiferromagnetic and ferromagnetic interactions leading to a clear ferrimagnetic transition in cobalt–molybdenum phosphate systems. Further measurements are required to fully understand the behaviour and the role of the interactions.

4. Conclusion

We have isolated the first sandwich-type cobalt(II)–molybdenum(V) phosphate hybrid material containing an organic amine bound to an inorganic core of the structure. The material features a one-dimensional hybrid polymer which co-crystallises in the solid state with piperazinium cations and water molecules, with which it interacts through an extensive and rather complex hydrogen bonding network. This compound shows a paramagnetic behaviour from 150 K to room temperature due to the spin only contribution from the Co(II) centres. Below 150 K, a ferrimagnetic (or weak ferromagnet) behaviour with critical temperature of 10 K was observed, which suggests magnetic interactions between the Co(II) ions probably mediated by the hexa-Mo rings.

Acknowledgments

We are grateful to FEDER, POCTI (Portugal), and to the Portuguese Foundation for Science and Technology (FCT) for their general financial support and also to the postdoctoral research Grant No. SFRH/BPD/9309/2002 (to F.-N.S.). P.G. also thanks FCT for the Ph.D. Grant No. SFRH/BD/17968/2004.

Appendix A. Supplementary materials

Supplementary data associated with this article can be found in the online version at doi:10.1016/j.jssc.2006.02.001.

References

[1] Z.T. Yu, Z.L. Liao, Y.S. Jiang, G.H. Li, G.D. Li, J.S. Chen, Chem. Commun. (2004) 1814–1815;
E.V. Anokhina, A.J. Jacobson, J. Am. Chem. Soc. 126 (2004) 3044–3045;
M.P. Kapoor, A. Bhaumik, S. Inagaki, K. Kuraoka, T. Yazawa, J. Mater. Chem. 12 (2002) 3078–3083.

[2] N.L. Rosi, J. Eckert, M. Eddaoudi, D.T. Vodak, J. Kim, M. O'Keeffe, O.M. Yaghi, Science 300 (2003) 1127–1129;
S. Onishi, T. Ohmori, T. Ohkubo, H. Noguchi, L. Di, Y. Hanzawa, H. Kanoh, K. Kaneko, Appl. Surf. Sci. 196 (2002) 81–88;
M. Eddaoudi, J. Kim, N. Rosi, D. Vodak, J. Wachter, M. O'Keefe, O.M. Yaghi, Science 295 (2002) 469–472.

[3] F. Caruso, R.A. Caruso, H. Mohwald, Science 282 (1998) 1111–1114.

[4] B. Julian, R. Corberan, E. Cordoncillo, P. Escribano, B. Viana, C. Sanchez, J. Mater. Chem. 14 (2004) 3337–3343;
E. Dujardin, S. Mann, Adv. Mater. 16 (2004) 1125–1129;
B. Zhao, P. Cheng, X.Y. Chen, C. Cheng, W. Shi, D.Z. Liao, S.P. Yan, Z.H. Jiang, J. Am. Chem. Soc. 126 (2004) 3012–3013;
B. Zhao, P. Cheng, Y. Dai, C. Cheng, D. Liao-Zheng, S.P. Yan, Z.H. Jiang, G.L. Wang, Angew. Chem. Int. Ed. 42 (2003) 934;
C.G. Barry, E.C. Turney, C.S. Day, G. Saluta, G.L. Kucera, U. Bierbach, Inorg. Chem. 41 (2002) 7159–7169;
X.L. Wang, Z.H. Kang, E.B. Wang, C.W. Hu, J. Electroanal. Chem. 523 (2002) 142–149;
C. Bellitto, F. Federici, Inorg. Chem. 41 (2002) 709–714;
M.C. Hong, Chin. J. Inorg. Chem. 18 (2002) 24–26;
C. Bellitto, F. Federici, A. Altomare, R. Rizzi, S.A. Ibrahim, Inorg. Chem. 39 (2000) 1803–1808;
K. Fegy, N. Sanz, D. Luneau, E. Belorizky, P. Rey, Inorg. Chem. 37 (1998) 4518–4523.

[5] P. Gomez-Romero, Adv. Mater. 13 (2001) 163–174;
N. Mizuno, M. Misono, Chem. Rev. 98 (1998) 199–217;
E. Coronado, C.J. Gómez-García, Chem. Rev. 98 (1998) 273–296.

[6] R.C. Haushalter, L.A. Mundi, Chem. Mater. 4 (1992) 31–48.

[7] H.X. Guo, S.X. Liu, Inorg. Chem. Commun. 7 (2004) 1217–1220;
L.Y. Duan, F.C. Liu, X.L. Wang, E.B. Wang, C. Qin, Y.G. Li, X.L. Wang, C.W. Hu, J. Mol. Struct. 705 (2004) 15–20;
R.D. Huang, F.C. Liu, Y.G. Li, M. Yuan, E.B. Wang, G.H. De, C.W. Hu, N.H. Hu, H.Q. Jia, Inorg. Chim. Acta 349 (2003) 85–90;
M. Yuan, E.B. Wang, Y. Lu, Y.G. Li, C.W. Hu, N.H. Hu, H.Q. Jia, J. Solid State Chem. 170 (2003) 192–197;
M. Yuan, E.B. Wang, Y. Lu, Y.G. Li, C.W. Hu, N.H. Hu, H.Q. Jia, Inorg. Chem. Commun. 5 (2002) 505–508;
W.B. Yang, C.Z. Lu, C.D. Wu, S.F. Lu, D.M. Wu, H.H. Zhuang, J. Clust. Sci. 13 (2002) 43–54;
Y.S. Zhou, L.J. Zhang, H.K. Fun, J.L. Zuo, I.A. Razak, S. Chantrapromma, X.Z. You, New J. Chem. 25 (2001) 1342–1346;
Y.S. Zhou, L.J. Zhang, X.Z. You, S. Natarajan, Int. J. Inorg. Mater. 3 (2001) 373–379;
Y.S. Zhou, L.J. Zhang, X.Z. You, S. Natarajan, J. Solid State Chem. 159 (2001) 209–214;
L. Xu, Y. Sun, E. Wang, E. Shen, Z. Liu, C. Hu, Y. Xing, Y. Lin, H. Jia, J. Mol. Struct. 519 (2000) 55–59;
L. Xu, Y.Q. Sun, E.B. Wang, E.H. Shen, Z.R. Liu, C.W. Hu, Y. Xing, Y.H. Lin, H.Q. Jia, New J. Chem. 23 (1999) 1041–1044;
A. Leclaire, A. Guesdon, F. Berrah, M.M. Borel, B. Raveau, J. Solid State Chem. 145 (1999) 291–301;
A. Guesdon, M.M. Borel, A. Leclaire, B. Raveau, Chem. Eur. J. 3 (1997) 1797–1800;
L.A. Meyer, R.C. Haushalter, Inorg. Chem. 32 (1993) 1579–1586.

[8] X. He, P. Zhang, T.Y. Song, Z.C. Mu, J.H. Yu, Y. Wang, J.N. Xu, Polyhedron 23 (2004) 2153–2159;
Y.H. Sun, X.B. Cui, J.Q. Xu, L. Ye, Y. Li, J. Lu, H. Ding, H.Y. Bie, J. Solid State Chem. 177 (2004) 1811–1816;
L. Xu, Y.Q. Sun, E.B. Wang, E.H. Shen, Z.R. Liu, C.W. Hu, Y. Xing, Y.H. Lin, H.Q. Jia, Transit. Met. Chem. 24 (1999) 492–495.

[9] F.A.A. Paz, J. Klinowski, J. Solid State Chem. 177 (2004) 3423–3432;
F.A.A. Paz, F.N. Shi, J. Klinowski, J. Rocha, T. Trindade, Eur. J. Inorg. Chem. (2004) 2759–2768;
F.A.A. Paz, J. Klinowski, Inorg. Chem. 43 (2004) 3882–3893;
F.A.A. Paz, J. Klinowski, Inorg. Chem. 43 (2004) 3948–3954;
F.A.A. Paz, J. Klinowski, J. Phys. Org. Chem. 16 (2003) 772–782;
F.A.A. Paz, J. Klinowski, Chem. Commun. (2003) 1484–1485;
F.A.A. Paz, A.D. Bond, Y.Z. Khimyak, J. Klinowski, Acta Crystallogr. C 58 (2002) M608–M610;
F.A.A. Paz, A.D. Bond, Y.Z. Khimyak, J. Klinowski, Acta Crystallogr. E 58 (2002) M691–M693;
F.A.A. Paz, Y.Z. Khimyak, A.D. Bond, J. Rocha, J. Klinowski, Eur. J. Inorg. Chem. (2002) 2823–2828.

[10] F.L. Sousa, F.A.A. Paz, C. Granadeiro, A.M.V. Cavaleiro, J. Rocha, J. Klinowski, H.I.S. Nogueira, Inorg. Chem. Commun. 8 (2005) 924–927;
F.L. Sousa, F.A.A. Paz, A.M.V. Cavaleiro, J. Klinowski, H.I.S. Nogueira, Chem. Commun. 3 (2004) 2656–2657;
F.N. Shi, Y. Xu, J.F. Bai, X.Z. You, Inorg. Chem. Commun. 2 (1999) 572–575.

[11] C.L. Pan, J.F. Song, J.Q. Xu, G.H. Li, L. Ye, T.G. Wang, Inorg. Chem. Commun. 6 (2003) 535–538.

[12] T. Kottke, D. Stalke, J. App. Crystallogr. 26 (1993) 615–619.

[13] R. Hooft, Collect: Data Collection Software, Nonius BV, Delft, The Netherlands, 1998.

[14] Z. Otwinowski, W. Minor, in: C.W. Carter Jr., R.M. Sweet (Eds.), Methods in Enzymology, Academic Press, New York, 1997, p. 307.

[15] R.H. Blessing, Acta Crystallogr. A 51 (1995) 33–38;
R.H. Blessing, J. Appl. Crystallogr. 30 (1997) 421.

[16] G.M. Sheldrick, SHELXS-97, Program for Crystal Structure Solution, University of Göttingen, 1997.

[17] G.M. Sheldrick, SHELXL-97, Program for Crystal Structure Refinement, University of Göttingen, 1997.

[18] C. du Peloux, P. Mialane, A. Dolbecq, J. Marrot, E. Rivière, F. Sécheresse, J. Mater. Chem. 11 (2001) 3392–3396.

[19] M.J. Manos, A.D. Keramidas, J.D. Woollins, A.M.Z. Slawin, T.A. Kabanos, J. Chem. Soc. Dalton Trans. (2001) 3419–3420.

[20] Y.S. Zhou, L.J. Zhang, X.Z. You, S. Natarajan, Inorg. Chem. Commun. 4 (2001) 699–704;
C. du Peloux, P. Mialane, A. Dolbecq, J. Marrot, F. Varret, F. Sécheresse, Solid State Sci. 6 (2004) 719–724.

[21] G. Cao, R.C. Haushalter, K.G. Strohmaier, Inorg. Chem. 32 (1993) 127–128.

[22] M.J. Manos, J.D. Woollins, A.M.Z. Slawin, T.A. Kabanos, Angew. Chem. Int. Ed. 41 (2002) 2801.

[23] C. Livage, E. Dumas, C. Marchal-Roch, G. Hervé, C.R. Acad. Sci. Ser. II C 3 (2000) 95–100.

[24] M.T. Pope, Heteropoly and Isopoly Oxometalates, Springer, New York, 1983.

[25] A. Müller, P. Kögerler, A.W.M. Dress, Coord. Chem. Rev. 222 (2001) 193–218;
A. Müller, S. Polarz, S.K. Das, E. Krickemeyer, H. Bögge, M. Schmidtmann, B. Hauptfleisch, Angew. Chem. Int. Ed. 38 (1999) 3241–3245.

[26] J.S. Griffith, The Theory of Transition-Metal Ions, Cambridge University Press, Cambridge, 1971.

[27] O. Kahn, Molecular Magnetism, Wiley-VCH, 1993.

[28] B. Barbara, D. Gignoux, C. Vettier, Lectures on Modern Magnetism, Science Press and Springer, 1988.

[29] R. Boca, Theoretical Foundations of Molecular Magnetism, Elsevier, Lausanne, 1999.